Design and Control of Modular Multilevel Converters for Battery Electric Vehicles

Mahran Quraan, Taejung Yeo, and Pietro Tricoli, *Member, IEEE*

***Abstract*—New advanced power conversion systems play an essential role in the extension of range and life of batteries. This paper proposes a new modular multilevel converter with embedded electrochemical cells that achieves very low cell unbalancing without traditional balancing circuits and a negligible harmonic content of the output currents. In this new topology, the cells are connected in series by means of half-bridge converters, allowing high flexibility for the discharge and recharge of the battery. The converter features a cell balancing control that operates on each individual arm of the converter to equalize the state of charge of the cells. The paper shows that the proposed control does not affect the symmetry of the three-phase voltage output, even for significantly unbalanced cells. The viability of the proposed converter for battery electric vehicles and the effectiveness of the cell balancing control are confirmed by numerical simulations and experiments on a kilowatt-size prototype.**

***Index Terms*—Battery electric vehicles (BEVs), modular multilevel converters (MMCs), state-of-charge balancing, traction drives.**

I. Introduction

THE private transport sector has been growing steadily over the recent years with about 20 million vehicles produced in Europe in 2013 [1]. The technological improvement of traditional internal combustion engines does not seem to be enough to solve the issues related to the carbon footprint of road vehicles. Therefore, the long-term sustainability of mobility can be ensured only if new technologies are effectively introduced into the market. Battery electric vehicles (BEVs) are an attractive alternative to conventional cars due to their zero emissions and lower environmental impact. However, BEVs are a less mature technology with still large margins for improvements, especially in the area of energy storage devices and electric drives.

At present, the standard topology of the power train for BEVs is based on a two-level inverter fed by a battery pack [2], [3]. Low-voltage battery cells (e.g. 2–4 V) are connected in series to reach the voltage required by the inverter (e.g., 150–300 V). The series connection implies the same current for all the cells, but differences in leakage currents and in cell construction can lead to an inhomogeneous voltage distribution across the cells and to an unequal state of charge (SOC). Therefore, some cells may be completely discharged much earlier than others, preventing any further use of the battery pack and effectively reducing the distance range of the BEV. Moreover, the unbalancing of the cells can cause premature failure of the pack over extended cycling due to the over- or undercharging of cells. For this reason, passive or active battery management systems (BMSs) are normally added to the battery pack [4]. Passive BMSs dissipate the excess energy of the cells with higher SOC in shunt resistors for equalizing the cells voltage. This technique has the advantages of low cost and low complexity but presents high energy losses and a slow balancing rate (about 1% of the SOC per hour). By contrast, active BMSs redistribute energy between cells with circuits containing controllable switches. Active balancing by charge-shuttling elements employs flying capacitors that can be selectively connected to the cells with switches. Thus, the most charged cells are connected to the capacitors that act as energy buffers and are subsequently discharged into the least charged cells. Alternative active balancing circuits include coupled inductors as energy buffer devices or dc–dc converters [5]. Generally, active balancing methods can provide a faster balancing rate and higher efficiency but increase the complexity and the cost of the BMS [5].

Many traction drives for BEVs use a standard bidirectional dc–dc boost converter to interface the battery pack to the dc-link of the traction inverter; the main purpose of the boost converter is to reduce the number of cells connected in series. However, this boost converter uses an inductor rated for the full power of the battery pack that increases the overall weight and reduces the efficiency. Moreover, the inductor losses limit the operating temperature [6].

These problems could be overcome by a new topology for the traction drive based on modular multilevel converters (MMCs) with embedded electrochemical cells. Unlike conventional MMCs, the power sources are inside the submodule (SMs). MMCs can be successfully used as motor drives of BEVs because they offer a low total harmonic distortion (THD) of output voltages and currents and high efficiency of the cell balancing. Due to the high number of levels, MMCs do not require a high switching frequency to supply nearly sinusoidal currents, and the voltage endured by each semiconductor switch is also significantly smaller than conventional converters. Modular concepts could improve converter's performances by giving more flexibility on the energy management and fault-tolerance capabilities [7], [8]. The proposed MMC has dc busbars that can be used for powering the auxiliary loads of the vehicles and the balancing algorithm does not require the introduction of zero-sequence components on the arms voltages.

Manuscript received September 16, 2014; revised January 4, 2015; accepted February 17, 2015. Date of publication March 3, 2015; date of current version September 21, 2015. This work was supported by the Samsung Advanced Institute of Technology under the Global Research Outreach Program 2012. Recommended for publication by Associate Editor M. Ferdowsi.

M. Quraan and P. Tricoli are with the School of Electronic, Electrical and Computer Engineering–University of Birmingham, Birmingham B15 2TT, U.K. (e-mail: msq266@bham.ac.uk; p.tricoli@bham.ac.uk).

T. Yeo is with the Samsung Advanced Institute of Technology, Gyeonggi-do 443-803, Korea, (e-mail: p.tricoli@bham.ac.uk).

Color versions of one or more of the figures in this paper are available online at http://ieeexplore.ieee.org.

Digital Object Identifier 10.1109/TPEL.2015.2408435

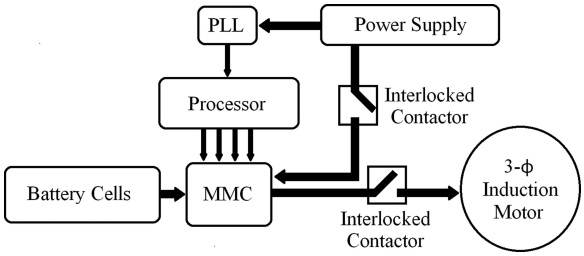

Fig. 1. System block diagram.

In this paper, a converter structure based on a double-star half-bridge converter is examined; cell balancing is obtained by a control strategy based on applying cluster, arm, and individual SOC-balancing controllers. Those controllers actively equalize the SOC of the cells, thus embedding the function of a BMS directly in the converter. Moreover, the converter can potentially increase the vehicle availability since it can tolerate failures even if they involve more than one module. In comparison with the cascaded H-bridge converter (CHB), which is usually based on two sets of star-configured converters in which the ac sides of multiple H-bridge cells are cascaded to constitute each arm [9], the proposed converter has the same number of switches, because each module is a half-bridge converter instead of a full-bridge converter. In order to get the same voltage across the motor, the number of modules of an MMC is double than that of a CHB, but with one-half capacity of the battery cells. Moreover, the MMC topology allows the recharge of the electrochemical cells either from dc or ac power sources, single-phase or three-phase, which is not possible for CHBs. The converter is controlled by a carrier disposition—sinusoidal pulse width modulation (SPWM), which is used to separately control each phase-leg of the MMC and to obtain symmetric three-phase output voltages [10]. When the converter is connected to the ac mains, a phase-locked loop is used to estimate the frequency and the phase of the grid voltage [11]. The controller of the converter is also responsible for balancing the SOC and all the battery cells and recharging the cells at nearly unity power factor.

This paper presents the fundamental capabilities of the proposed MMC used both as a traction converter and a BMS. A first prototype of MMC with embedded lithium-ion cells has been designed and tested to verify the validity of the theoretical results and the performance of the balancing algorithm. This prototype has not been optimized to fit into a real car yet, and the SMs have been designed with a natural air cooling. Future work on a more compact converter will include a more advanced cooling system and a thermal management of the cells. The thermal management can be easily included in the proposed controller, because the cells can be individually connected or disconnected by the half-bridge converters if the temperature is outside an optimal band.

II. Converter Structure and Operation Principle

The block diagram of the traction system of BEV is shown in Fig. 1. The MMC can be connected to the traction motor or an external ac power supply via an interlocked switch to enable motoring of recharge operations. The layout of the proposed MMC is represented in the schematic of Fig. 2, where the SMs consist of a single electrochemical cell with a half-bridge converter. Due to voltage level of SMs, low-voltage MOSFETs can be used as power switches to reduce conduction and switching losses of the converter. For this reason, fast switching antiparallel diodes are avoided and the body diodes of the MOSFETs conduct only during the dead-time between the commutations. The arms of the converter are connected by means of two uncoupled buffer inductors. The buffer inductors limit the current circulating between the legs of the converter. Alternatively, a single coupled inductor could be used for the same function [9], [12], [13]. With n SMs per arm, this converter generates $n+1$ levels of the line-to-line ac voltage. The voltage stress across each switching device is limited to the voltage of one electrochemical cell.

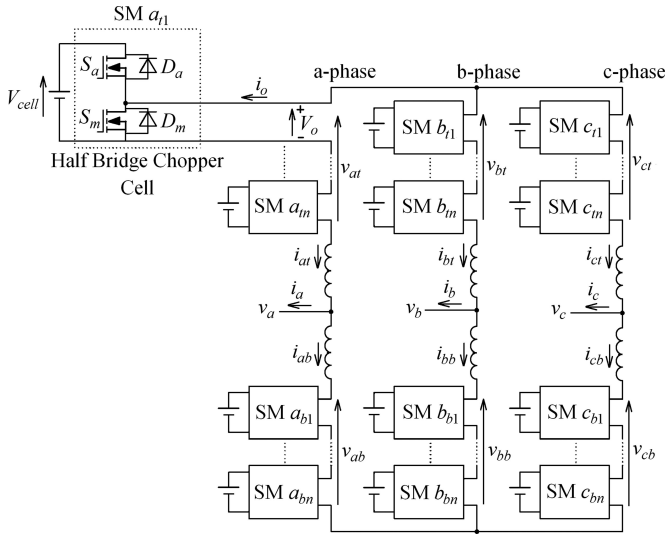

Fig. 2. Layout of the proposed MMC with electrochemical cells.

The operation principle of the bidirectional half-bridge chopper cell can be explained with reference to Fig. 2. When the switch S_a is turned ON, the output voltage V_0 is equal to the cell voltage $V_{\rm cell}$. The battery cell is discharged or recharged depending on the direction of the current i_o. If the switch S_m is turned ON instead, V_0 is equal to zero and the SOC of the cell is unchanged [14]. The maximum voltage on each arm is $V_{\rm arm,max} = nV_{\rm cell}$, being $V_{\rm cell}$ the nominal voltage of a single electrochemical cell and n the number of SMs for each arm. The two arms of each leg are controlled complementarily in order to keep constant the voltage between the positive and the negative busbars. Therefore, the two reference voltages for the top and bottom arms, $v_{{\rm ref},kt}$ and $v_{{\rm ref},kb}$, are

$$v_{{\rm ref},kt} = \frac{V_{\rm arm,max}}{2} - v_k, \quad v_{{\rm ref},kb} = \frac{V_{\rm arm,max}}{2} + v_k, \quad -\frac{V_{\rm arm,max}}{2} \le v_k \le \frac{V_{\rm arm,max}}{2} \tag{1}$$

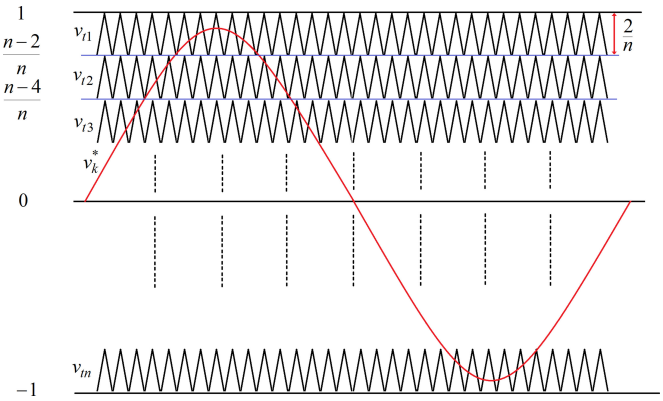

Fig. 3. Carrier disposition SPWM strategy.

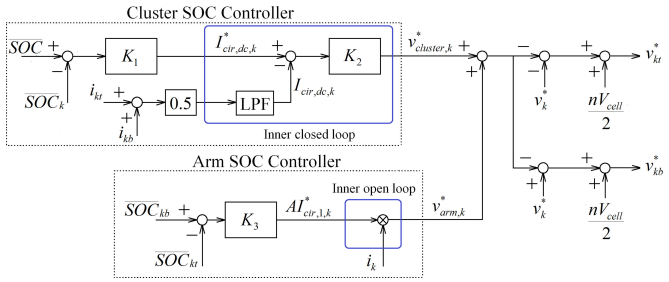

Fig. 4. Block diagram of cluster and arm SOC controller.

where v_k is the phase voltage and k is the phase, i.e., a, b, or c. Thus, the maximum amplitude value of phase voltage is $V_{k,\max} = V_{\text{arm},\max}/2$.

Due to the differences between the electrochemical cells, the three legs may have different voltages even with the same number of SMs turned-on and this would lead to uncontrolled current flowing through the arms that create additional losses and undesired harmonics [15], [16]. At the same time, circulating currents can be used to balance the cells without affecting motor currents. For this reason, it is essential to control the circulating current of the converter to maximize the efficiency of the cell balancing and minimize the power losses. For the MMC topology, the top and bottom arm currents of the phase k can be expressed as

$$i_{kt} = \frac{i_k}{2} + i_{\text{cir},k}, \quad i_{kb} = -\frac{i_k}{2} + i_{\text{cir},k} \tag{2}$$

where i_{kt} is the top arm current of phase k, i_{kb} is the bottom arm current of phase k, i_k is the phase k current, and $i_{\text{cir},k}$ is the circulating current that flows through the phase k. By solving (2), the circulating current of the phase k can be expressed as

$$i_{\text{cir},k} = \frac{i_{kt}}{2} + \frac{i_{kb}}{2}. \tag{3}$$

III. Control Strategy of the Converter

The controller of the converter has two main sections: the motor control and the SOC balancing control. The motor control is based on a standard vector control with field orientation on the rotor flux and produces the voltage references for the three phases v_k^*. These references are used by the sinusoidal PWM modulator to generate the pulses for the switches of the MOSFETs within the SMs [10]. The modulation technique is based on the carrier disposition strategy that uses n triangular carriers with the same frequency and amplitude but with an offset of $2/n$, as Fig. 3 shows. In the figure, the voltage is normalized to the voltage $V_{k,\max}$.

The SOC-balancing control of the cells per each SM is divided into the individual balancing, the arm balancing, and the cluster SOC-balancing control. These controls are explained in detail in the following sections. Fig. 4 shows the block diagram of both cluster and arm SOC-balancing controllers.

A. Individual Balancing Control

The individual balancing control takes the responsibility to keep all cells within the same arm at the same average SOC by sorting and selecting the active SMs without closed-loop controller. The reference SOC for the cells of the same arm is the average of the SOCs, which are indicated respectively with $\overline{\text{SOC}}_{kt}$ and $\overline{\text{SOC}}_{kb}$ for the top and bottom arm of phase k. In the individual SOC-balancing controller, the active SMs are sorted on the basis of the estimated SOC of the electrochemical cells. The sorting order is ascending or descending depending on the direction of the current in the arm. If the current discharges the cells, the active cells with the highest SOC are selected and vice versa [17], [18]. The priority algorithm forces the cells to balance because the active cells are always the outliers of the arm. The SOC of each cell is estimated by using the Coulomb counting method [18]–[20]

$$\begin{aligned} \text{SOC}_{h,kt}(t) &= \text{SOC}_{h,kt}(t_0) - \frac{1}{3600 Q_{max}} \left(\int_{t_0}^{t} i_{h,kt}(t)\, dt \right), \\ & h = 1, ..., n, \ k = a, b, c \\ \text{SOC}_{h,kb}(t) &= \text{SOC}_{h,kb}(t_0) - \frac{1}{3600 Q_{max}} \left(\int_{t_0}^{t} i_{h,kb}(t)\, dt \right), \\ & h = 1, ..., n, \ k = a, b, c, \end{aligned} \tag{4}$$

where $\text{SOC}_{h,kt}(t_0)$ and $\text{SOC}_{h,kb}(t_0)$ are the initial SOCs of the cell of top and bottom arms of phase k, $i_{h,kt}(t)$ and $i_{h,kb}(t)$ are the instantaneous currents flowing through the hth cell of the top and bottom arms of phase k, and $Q_{\max}$ is the rated capacity of the cells. In practice, the estimation of the SOC based only on the Coulomb counting method can lead to incorrect results due to difference between the cells, such as different leakage resistance, cell internal temperature, and aging. The proposed controller can take into account these phenomena by modifying (4) as follows:

1) The initial SOC values at time t_0 are updated by measuring the open-circuit voltage (OCV) of the cell when the electric vehicle is not in use; the relation between the OCV and SOC can be preliminary estimated according to [21].
2) The battery current needs to be multiplied by the coulombic efficiency to compensate for the energy losses occurring during the recharging process. This efficiency is a

function of the recharge current and can be preliminary estimated according to [22] and [23].

3) The rated capacity of the cell is a function of the cell's temperature and can be preliminary evaluated according to [22] and [23].

It is worth noting that not all the currents in (4) have to be measured. Due to the series connection of the modules, the current is the same in each SM of the same arm. Therefore, only two current sensors per leg are necessary and the current flowing in each cell can be calculated from the knowledge of the arm current and the switching function of the half-bridge converter

$$\begin{aligned} &i_{h,kt}\left(t\right)=i_{kt,}\ S_h, \quad h=1,...,n,\ k=a,b,c\\ &i_{h,kb}\left(t\right)=i_{kb,}\ S_h, \quad h=1,...,n,\ k=a,b,c\\ &S_h=\begin{cases}1, & \text{Top MOSFET is ON}\\ 0, & \text{Top MOSFET is OFF.}\end{cases}\end{aligned} \tag{5}$$

The individual controller is flexible and can be improved by adding a thermal management, which is essential when the converter has to be fitted in a real BEV. In this case, the temperatures of the cells are monitored to ensure that they remain within an optimal band that minimizes the degradation of the cells. Therefore, the cells with a temperature higher than a hot limit are excluded from the sorting algorithm and cool off because not in use. Once their temperature is below the hot limit plus a margin, the cells are included again and balanced with the others. Similarly, if the temperature is below a cold limit, the cells are active all the time and warm up until they reach the cold limit plus a set margin. This thermal control can be further accelerated by adding a flow management of the cooling agent of the battery cells.

B. Arm Balancing Control

The arm balancing control forces the cells of top and bottom arms within the same leg to have an average SOC equals to the average SOC of all the modules in the phase leg. The average SOCs of top and bottom arms of phase *k* are given by

$$\begin{pmatrix}\overline{\mathrm{SOC}}_{kt}\\ \overline{\mathrm{SOC}}_{kb}\end{pmatrix}=\frac{1}{n}\sum_{h=1}^{n}\begin{pmatrix}\mathrm{SOC}_{h,kt}\\ \mathrm{SOC}_{h,kb}\end{pmatrix}. \tag{6}$$

Ignoring the switching losses of the half-bridge converters, the instantaneous powers of top and bottom arms of each phase leg can be expressed as (see the Appendix)

$$\begin{aligned} p_{kt} &= v_{kt}i_{kt}=n\,Q_{\max}V_{\mathrm{cell}}\frac{d\overline{\mathrm{SOC}}_{kt}}{dt}\\ &= \left(\frac{nV_{\mathrm{cell}}}{2}-v_k-L\frac{di_{kt}}{dt}\right)i_{kt}\\ p_{kb} &= v_{kb}i_{kb}=n\,Q_{\max}V_{\mathrm{cell}}\frac{d\overline{\mathrm{SOC}}_{kb}}{dt}\\ &= \left(\frac{nV_{\mathrm{cell}}}{2}+v_k-L\frac{di_{kb}}{dt}\right)i_{kb}\end{aligned} \tag{7}$$

where v_{kt} and v_{kb} are the arm voltages and *L* is the inductance of the buffer inductors. The differential instantaneous power of each phase-leg is given by

$$\begin{aligned} p_{k,\mathrm{diff}} &= p_{kt}-p_{kb}\\ &= n\,Q_{\max}\,V_{\mathrm{cell}}\frac{d\left(\overline{\mathrm{SOC}}_{kt}-\overline{\mathrm{SOC}}_{kb}\right)}{dt}\\ &= -\frac{1}{2}n\,V_{\mathrm{cell}}i_k-2v_ki_{\mathrm{cir},k}-L\frac{d\left(i_ki_{\mathrm{cir},k}\right)}{dt}.\end{aligned} \tag{8}$$

Assuming sinusoidal voltage and current for the load

$$v_k=V_k\sin\left(\omega t\right),\quad i_k=I_k\sin\left(\omega t-\phi\right) \tag{9}$$

expanding the circulating current with the Fourier series

$$i_{\mathrm{cir},k}=I_{\mathrm{cir,dc},k}+\sum_{j=1}^{\infty}I_{\mathrm{cir},j,k}\sin\left(j\omega t+\theta_j\right) \tag{10}$$

substituting (9) and (10) into (8), and neglecting the alternating terms, the differential power is given by

$$p_{k,\mathrm{diff}}=n\,Q_{\max}\,V_{\mathrm{cell}}\frac{d\left(\overline{\mathrm{SOC}}_{kt}-\overline{\mathrm{SOC}}_{kb}\right)}{dt}\cong-V_kI_{\mathrm{cir},1,k}\cos\theta_1. \tag{11}$$

Equation (11) shows that only the fundamental component of the circulating current is useful to balance the SOC between the top and bottom arms. The reference for the amplitude of fundamental component of circulating current, $I^*_{\mathrm{cir},1,k}$, is given by the output of the proportional controller that amplifies the difference between $\overline{\mathrm{SOC}}_{kt}$ and $\overline{\mathrm{SOC}}_{kb}$.

In this paper, the calculation of the phase of the fundamental component of the circulating current is open loop to simplify the design and avoid proportional-resonant controllers. The output given by the arm SOC controller is denoted by $v^*_{\mathrm{arm},k}$ and represents the reference voltage drop across buffer inductor caused by the fundamental component of the circulating current

$$\begin{aligned} v^*_{\mathrm{arm},k} &= L\frac{d}{dt}\left[I^*_{\mathrm{cir},1,k}\sin\left(\omega t+\theta_1\right)\right]\\ &= -\omega\,L\,I^*_{\mathrm{cir},1,k}\sin\left(\omega t-\frac{\pi}{2}+\theta_1\right).\end{aligned} \tag{12}$$

Assuming $\phi=\pi/2-\theta_1$, which is valid at steady state, (12) becomes

$$v^*_{\mathrm{arm},k}=-\frac{\omega L}{I_k}I^*_{\mathrm{cir},1,k}i_k=AI^*_{\mathrm{cir},1,k}i_k. \tag{13}$$

Fig. 4 shows a block diagram of the *k*-phase arm SOC-balancing control, where $v^*_{\mathrm{arm},k}$ is the voltage command obtained from the balancing control

$$v^*_{\mathrm{arm},k}=K_3\left(\overline{\mathrm{SOC}}_{kb}-\overline{\mathrm{SOC}}_{kt}\right)\ i_k. \tag{14}$$

Rearranging (11)

$$\frac{d\left(\overline{\mathrm{SOC}}_{kt}-\overline{\mathrm{SOC}}_{kb}\right)}{dt}=-\frac{V_k\sin\phi}{nV_{\mathrm{cell}}Q_{\max}}I_{\mathrm{cir},1,k}=BI_{\mathrm{cir},1,k} \tag{15}$$

the transfer function of the arm controller is given by

$$\frac{\overline{\mathrm{SOC}}^*_{kt}\left(s\right)-\overline{\mathrm{SOC}}^*_{kb}\left(s\right)}{\overline{\mathrm{SOC}}_{kt}\left(s\right)-\overline{\mathrm{SOC}}_{kb}\left(s\right)}=\frac{B\,K_3}{B\,K_3+A\,s} \tag{16}$$

which can be used to design the gain K_3.

C. Cluster Balancing Control

The cluster balancing control is responsible for forcing the *k*-phase average SOC, $\overline{\mathrm{SOC}}_k$, to the average SOC of the three phases [19]

$$\overline{\mathrm{SOC}} = \frac{\overline{\mathrm{SOC}}_a + \overline{\mathrm{SOC}}_b + \overline{\mathrm{SOC}}_c}{3} \tag{17}$$

where

$$\begin{pmatrix} \overline{\mathrm{SOC}}_a \\ \overline{\mathrm{SOC}}_b \\ \overline{\mathrm{SOC}}_c \end{pmatrix} = \frac{1}{2n} \sum_{h=1}^{n} \begin{pmatrix} \mathrm{SOC}_{h,at} + \mathrm{SOC}_{h,ab} \\ \mathrm{SOC}_{h,bt} + \mathrm{SOC}_{h,bb} \\ \mathrm{SOC}_{h,ct} + \mathrm{SOC}_{h,cb} \end{pmatrix} \tag{18}$$

.

The cluster balancing control operates on the dc component of the circulating currents only and it is not affected by the value of the phase currents. As shown in Fig. 4, the reference for the dc component of the circulating current of generic phase *k* is obtained using the following equation:

$$I^*_{\mathrm{cir,dc},k} = K_1 \left(\overline{\mathrm{SOC}} - \overline{\mathrm{SOC}}_k \right). \tag{19}$$

Using (7), the total instantaneous power of each phase-leg is given by

$$\begin{aligned} p_{k,\mathrm{total}} &= p_{kt} + p_{kb} = 2n\, Q_{\max}\, V_{\mathrm{cell}} \frac{d\overline{\mathrm{SOC}}_k}{dt} \\ &= -v_k i_k + n\, V_{\mathrm{cell}} i_{\mathrm{cir},k} - L \left(i_{kt} \frac{di_{kt}}{dt} + i_{kb} \frac{di_{kb}}{dt} \right). \end{aligned} \tag{20}$$

By substituting (9) and (10) into (20) and neglecting the alternating term, the previous equation becomes

$$\begin{aligned} p_{k,\mathrm{total}} &= 2n\, Q_{\max}\, V_{\mathrm{cell}} \frac{d\overline{\mathrm{SOC}}_k}{dt} \\ &\cong n\, V_{\mathrm{cell}} I_{\mathrm{cir,dc},k} - \frac{1}{2} V_k I_k \cos\phi. \end{aligned} \tag{21}$$

Equation (21) shows that the dc component of the circulating current can be used to balance the SOC between the three legs of the converter. Therefore, the voltage command obtained from the cluster control, $v^*_{\mathrm{cluster},k}$, is given by

$$\begin{aligned} v^*_{\mathrm{cluster},k} &= K_2 \left(I^*_{\mathrm{cir,dc},k} - I_{\mathrm{cir,dc},k} \right) \\ &= K_2 \left[K_1 \left(\overline{\mathrm{SOC}} - \overline{\mathrm{SOC}}_k \right) - I_{\mathrm{cir,dc},k} \right]. \end{aligned} \tag{22}$$

If $D(s)$ is $\frac{1}{2} V_k I_k \cos\phi$, the closed-loop transfer function of the cluster controller is given by

$$\begin{aligned} \overline{\mathrm{SOC}}_k(s) &= \frac{K_1}{K_1 + 2\, Q_{\max}\, s} \overline{\mathrm{SOC}}(s) \\ &\quad - \frac{1}{n\, V_{\mathrm{cell}}} \frac{1}{K_1 + 2\, Q_{\max}\, s} D(s) \end{aligned} \tag{23}$$

which can be used to design the gain K_1. The closed-loop transfer function of the dc component of the circulating current is given by

$$\frac{I^*_{\mathrm{cir,dc},k}(s)}{I_{\mathrm{cir,dc},k}(s)} = \frac{K_2}{K_2 + L\, s} \tag{24}$$

which can be used to design the gain K_2.

If the gains K_1, K_2, and K_3 are increased, the system responds faster to a change of the set-points and the steady-state errors are smaller. However, both cluster and arm SOC controllers generate a reference for the dc and fundamental components of the circulating currents. Therefore, an increase of the gains will result in a higher value of the circulating currents that reduce the output voltage of the converter. Therefore, both controllers have been saturated with an antiwindup to a level producing a voltage output equal to 5% of the nominal voltage.

As a result of the arm balancing control and the cluster control, the reference voltages of both top and bottom arms of phase *k* are obtained as

$$\begin{aligned} v^*_{kt} &= v^*_{\mathrm{cluster},k} + v^*_{\mathrm{arm},k} - v^*_k + \tfrac{nV_{\mathrm{cell}}}{2} \\ v^*_{kb} &= v^*_{\mathrm{cluster},k} + v^*_{\mathrm{arm},k} + v^*_k + \tfrac{nV_{\mathrm{cell}}}{2}. \end{aligned} \tag{25}$$

IV. Converter Reliability

Traditional two-level inverters have six power switches and all of them are required to operate the converter. For simplicity, the controlled switch and the diode are considered as a sole element with the same reliability. If *p* is the static reliability of a single switch [24], the reliability of the two-level inverter is given by

$$R = p^6. \tag{26}$$

For the MMC, the fault of one switch does not compromise the entire converter, because the faulty cell can be bypassed and the faulty arm will have $n-1$ levels instead of *n*. Therefore, the converter can keep working with an unbalance of the output voltages. Alternatively, the converter can keep working with balanced output voltage but with lower amplitude, operating all the arms with $n-1$ levels. Therefore, the reliability of the converter is a function of the power output required. In particular, if the nominal power of the converter is P_n and the power required is in the range $(k-1)\, P_n/n \le P \le kP_n/n$, at least *k* SMs must be healthy in the arm and each of them requires both the switches healthy. Therefore, from the theory on partial redundancy, the static reliability of the MMC is

$$R = \left(\sum_{i=k}^{n} \binom{n}{i} \left(p^2\right)^i \left(1-p^2\right)^{n-i} \right)^6 \tag{27}$$

The two reliabilities have been compared to understand the effect of the presence of redundancies in MMCs, selecting a number of level $n = 45$. The results are shown in Fig. 5 for a value of $p = 0.99$.

The figure clearly shows that the reliability of MMCs is greater than that of two-level inverters for a large range of the output power. When the full power is required, all the levels must be working, and therefore, the reliability of MMC is lower, due to the higher number of switches. For a low value of switches' reliability, MMCs are superior up to a power of 93%. For two-level inverters, the reliability of the converter is strongly affected by the reliability of the switches. For MMCs instead, the reliability is almost the same irrespective of the value of *p*, at least for a large range of the output power. Finally, it is worth to

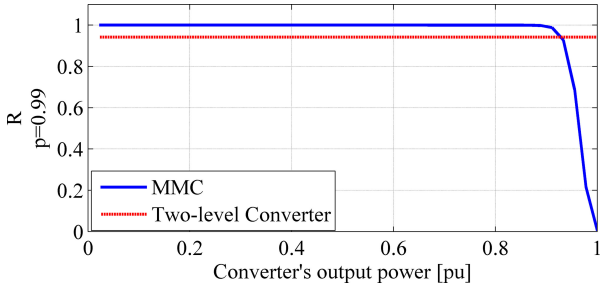

Fig. 5. Reliability of two-level and modular multilevel converters.

TABLE I
CIRCUIT PARAMETERS USED FOR THE SIMULATIONS

Load active power	P	65 kW
Load power factor	$\cos\varphi$	0.848
Nominal line-line rms voltage	V_n	100 V
Nominal rms current	I_n	442 A
Nominal frequency	f_n	50 Hz
Arm inductor	L	60 μH
Nominal battery capacity	Q_{max}	20 Ah
Nominal battery voltage	V_{cell}	3.7 V
Control time step	T_s	100 μs
Number of cells per each arm	n	45
Proportional gain of current controller	K_1	25 A
Proportional gain of cluster controller	K_2	0.5 V/A
Proportional gain of arm controller	K_3	0.04 V

note that previous results have been carried out using for the MMC only the minimum number of SMs to provide the nominal voltage of the converter. By adding more cells in each arms than those strictly necessary, the reliability of the converter is improved and it is higher than that of a two-level converter for the entire power range when the redundancy is at least 9%, i.e., $n = 49$.

V. SIMULATION RESULTS

The operating characteristics of the proposed MMC with embedded battery cells have been tested by means of numerical simulations. Table I summarizes the circuit parameters and control gains used for simulation based on a MATLAB/Simulink computer program. The initial SOC of the cells has been randomly assigned with a maximum of 15% of unbalancing between the most and least charged cell.

The converter has 270 Li-ion cells, i.e., 45 cells for each arm. Being the nominal voltage of the single cell equals to 3.7 V, the maximum achievable phase voltage is 58 V rms, equivalent to a line-to-line voltage of 100 V rms. In order to increase the efficiency of the conversion system, a larger number of cells should be used, allowing the connection of higher voltage loads. Moreover, a larger number of cells would improve further the voltage waveforms in terms of harmonic content.

The battery cells have been simulated as ideal voltage sources, having their output voltages linearly dependent on their SOC. Assuming a maximum voltage of 4.2 V and a minimum voltage of 3.0 V, the actual cell voltages of top and bottom arms are

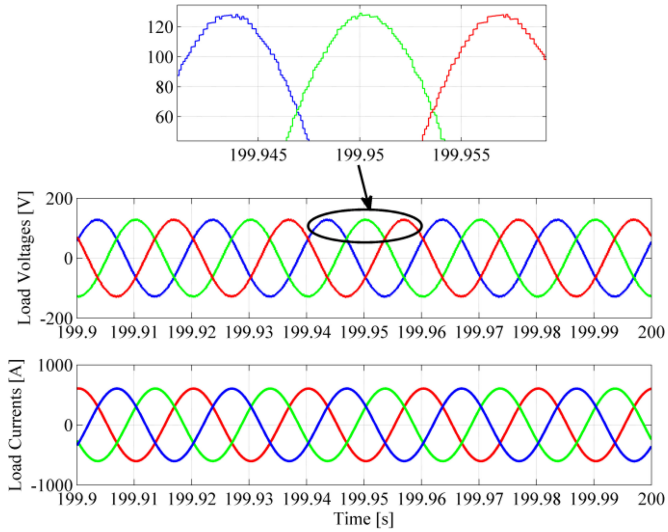

Fig. 6. Steady-state load voltages and currents.

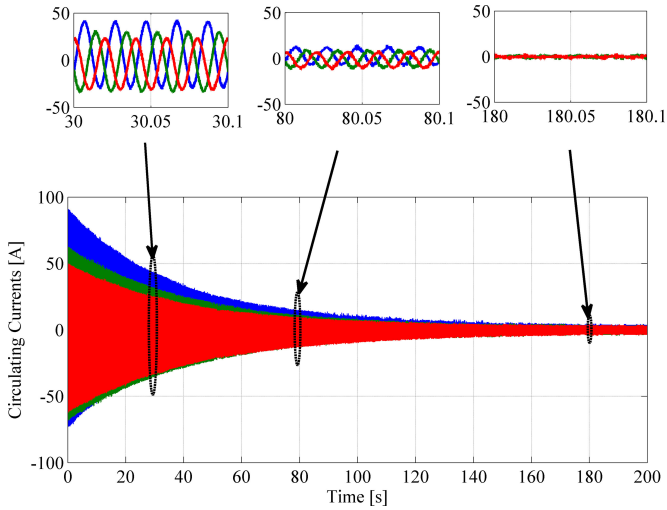

Fig. 7. Circulating currents due to the balancing algorithm.

given by the following equations:

$$v_{\text{cell},h,kt} = 3 + 1.2\,\text{SOC}_{h,kt}$$
$$v_{\text{cell},h,kb} = 3 + 1.2\,\text{SOC}_{h,kb}. \quad (28)$$

In order to take full advantage of the available levels, the control time step should be less than or equal to the period of the fundamental harmonic of the voltage over four times the number of levels [25]. The reference voltages of each arm are normalized by the nominal cell voltage V_{cell}. The reference voltages of the bottom arms lag the reference voltages of the top arms by an angle of 180°. The nearest integer of the normalized reference voltages of the arms is taken to determine the number of active modules in an arm.

Fig. 6 shows the load voltage and load current in the discharge mode of the cells. It is clear that the MMC produces output voltages with a very small THD (0.76%) and negligible distortion of the currents, due to the filtering effect of the load.

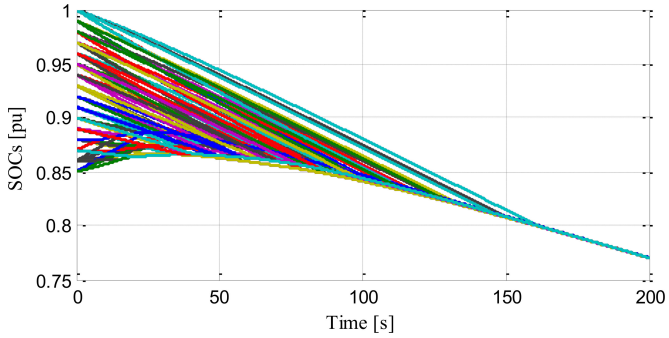

Fig. 8. SOCs of battery cells.

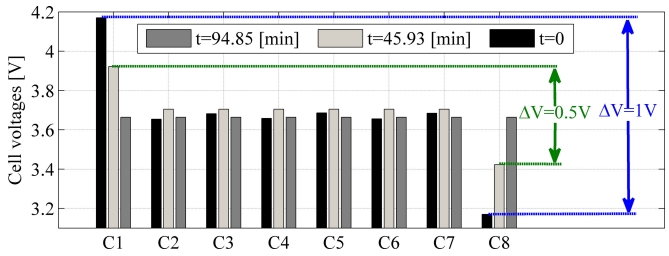

Fig. 9. Measured cell voltages at balancing time = 0, 45.93 min and 94.85 min.

The circulating currents are dependent on the level of unbalancing of the cells and have been calculated using (5). At the beginning of the simulation, the circulating currents are significant, because the three legs have different initial SOC averages. The cluster controller uses the circulating currents to balance the cells across different legs, and as shown from Fig. 7, the three circulating currents are not balanced. In steady-state condition, the cells of the different legs are balanced and the circulating currents are very small, as the same Fig. 7 shows. It is worth noting that the load currents are always balanced regardless of the SOC of the cells.

In Fig. 8, the SOC of all the 270 cells of the converter are reported. It is clear that, in the first part of the cycle, the cells with higher SOC discharge quicker, while the cells with lower SOC are recharged until all the cells have very similar SOC. With the proposed controller, all the cells are completely balanced after 160 s.

To verify the performance of the proposed converter, the equalizing time has been compared to the standard active cell balancing proposed in [26]. For the purpose of the comparison, the proposed converter has been tested with eight Li-ion batteries (4.2 V/10 Ah) per arm with a highly inductive load of 10 A. As in [26], the highest voltage of cell C1 is 4.17 V, the lowest voltage of cell C8 is 3.17 V, and the voltages of the remaining cells (C2–C7) are $\sim$ 3.67 V.

Fig. 9 shows that the voltage difference between cell 1 and cell 8 decreases from 1.0 to 0.5 V within 45.93 min compared to 180 min necessary for the BMS proposed in [26]. The reason of the very low equalization time of the proposed circuit is because the balancing current can be up to the full load current of the traction converter, without the limitations of the low-power balancing circuits of standard BMSs (equal to 6 A for the circuit in [26]). In the proposed converter, the circulating current can be designed according to the desired recharge current of the battery cells and the equalizing time. Fig. 10 shows that the proposed controller equalizes the SOCs of all battery cells without affecting the load voltages and currents.

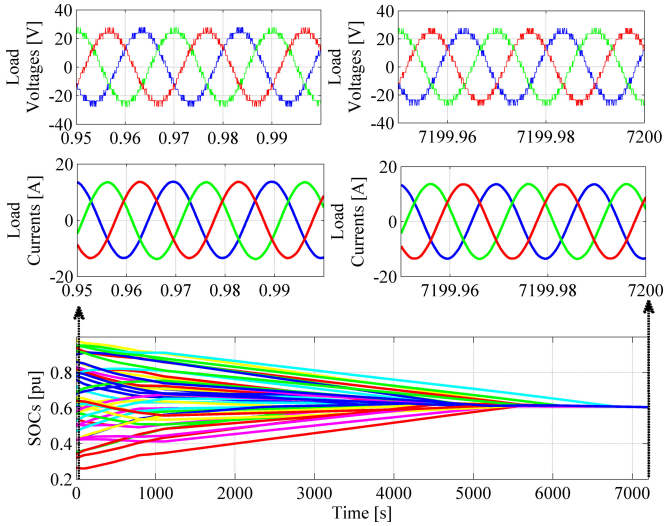

Fig. 10. SOCs of 48 cells, transient and steady-state load voltages and currents.

Fig. 11. Prototype of a five-level MMC with embedded lithium-ion batteries.

VI. Experimental Results

The proposed MMC has been experimentally tested on a small-scale laboratory prototype. In order to reduce the complexity of the circuit, a prototype with four modules per arm has been constructed, where each module has a lithium-ion cell as power source. A photograph of the five-level MMC built in the laboratory is shown in Fig. 11.

The control system is based on a NI CompactRIO, which combines an embedded real-time processor, a high-performance

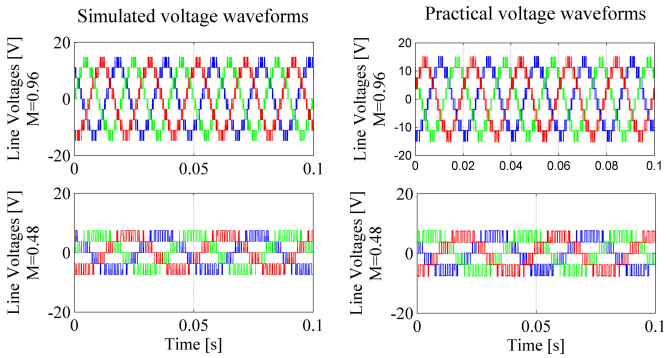

Fig. 12. Line-to-line voltage waveforms for different output voltages and frequencies.

field-programmable gate array (FPGA), and hot-swappable I/O modules. Both top and bottom arm currents are measured as input signals to the ADC unit. The FPGA unit has the following functions:

1) generation of the voltage commands v_k^*;
2) generation of the carrier signals with the appropriate carrier disposition SPWM technique;
3) comparison of v_k^* with the corresponding triangular carrier signals to determine the number of active SMs;
4) execution of the SOC balancing control algorithm.

Basically, traditional active BMSs have large number of low-current switches to balance the cells, typically 1–4 switches per each battery cell. For the proposed MMC, there are two high-current switches per battery cell. However, these switches have the same type of driver and transistor–transistor logic control; therefore, the controllability of the proposed converter has the same degree of complexity of state-of-the-art method BMS. On the other hand, modern FPGA can handle a large number of synchronized digital output signals required to modulate all SMs and achieve the SOC balancing for all battery cells used in the proposed MMC.

The converter is designed to drive the traction motor of the BEV, and hence, the number of active levels is dependent on the voltage amplitude required at the output terminals. Due to the modular design of the converter, the number of levels is easily adjusted by changing the modulation index and the voltage output is regulated by a SPWM of the last level. When a variable frequency is required, this control allows a quick variation of the voltage level in a way completely similar to traditional two-level inverters. In order to verify the experimental response of the converter to a variation of the output voltage and frequency, two tests have been made with a volt/hertz constant control at two modulation indices equal to 0.96 and 0.48 with the objective to evaluate the quality of the output voltage waveform in different conditions. The experimental tests have also been compared with the simulations. In the case of 0.96 modulation index, the switching frequency is 1 kHz and the fundamental frequency is 50 Hz, while in the case of 0.48 modulation index the switching frequency and fundamental frequency are 0.5 kHz and 25 Hz, respectively. Fig. 12 shows both simulated and experimental line-to-line voltages for the two output frequencies:

TABLE II
THD OF THE CONVERTER

N-level	THD[%](practical results)	THD[%](simulation results)
3	38.21	37.39
5	17.70	17.21

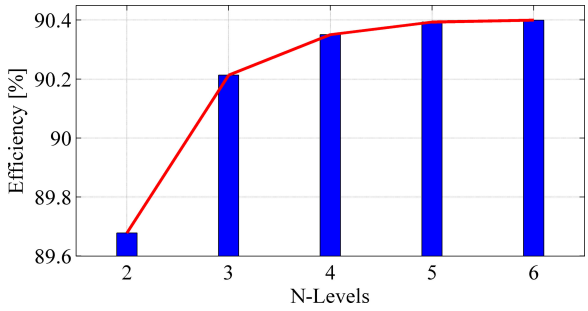

Fig. 13. Motor efficiency for different number of converter levels. Note: in all conditions, motor power 4 kW, voltage 400 V, frequency 50 Hz, speed 1430 rpm.

TABLE III
MOTOR ELECTRIC DATA

Nominal power [kW]	Nominal voltage [V]	Nominal motor current [A]	Pole Pairs	Nominal Speed [rpm]
0.55	400	1.34	2	1435

TABLE IV
CONVERTER PARAMETERS USED FOR EXPERIMENT

Nominal battery capacity [Ah]	Nominal battery voltage [V]	Nominal converter current [A]	Arm inductor [μH]	Switching frequency [kHz]
10	3.7	50	22	1.05

the larger number of levels, the smaller THD of output voltage. Table II compares the results between the simulation and the experiment based on THD. Both results show a close agreement and highlight the small distortion attained with the proposed MMC. Therefore, losses of traction motor are also significantly reduced. In order to quantify the improvement of motor efficiency with a higher number of levels, a simulation has been carried out running an induction motor with the same voltage amplitude and frequency and with the same torque. The result is shown in Fig. 13, where it is evident that an increment of the efficiency of about 0.8% has to be expected, with a significant impact in the driving efficiency of the BEV.

The converter has been experimentally tested with an induction motor, whose data given in Table III. A 10-V/400-V 1.2-kVA three-phase transformer has been used to boost the converter voltage to the level suitable for the motor. Table IV

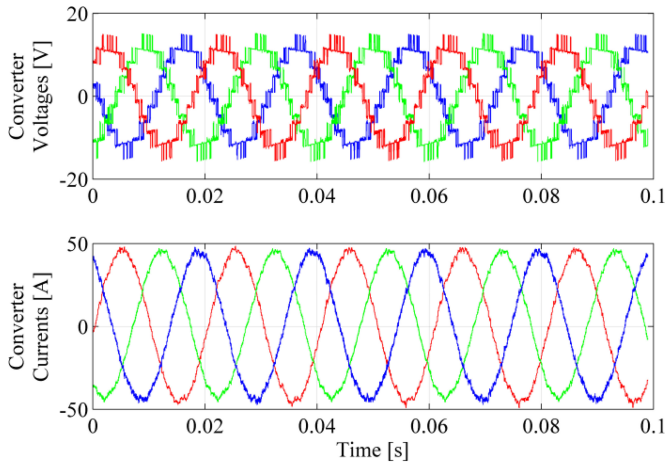

Fig. 14. Converter output voltages and current.

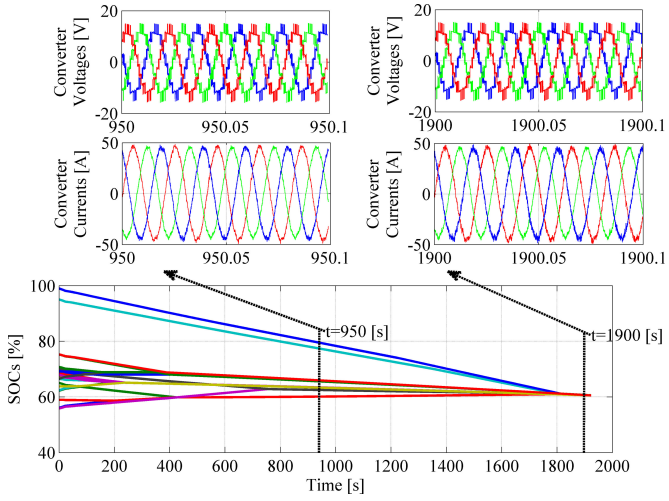

Fig. 15. SOCs of the 24 battery cells, output voltages, and currents at 950 and 1900 s.

summarizes the circuit and battery parameters used for experiment. To fully validate the SOC balance capability of the proposed MMC, the initial imbalance of the SOC has been set to 44%. Fig. 14 shows the output voltages and currents at nominal motor speed. It is clear that the MMC produces output currents with a very small THD, due to the filtering effect of the motor. The small imbalance of the current is due to the asymmetry of the windings of the induction motor. Fig. 15 shows the SOCs of all battery cells and the converter output voltages and currents measured at $t = 950$ s and $t = 1900$ s in order to demonstrate that they are not affected by the balancing control. From the experimental results, it is clear that controller equalizes the SOCs of all battery cells toward the same level even if the cells have a large initial unbalancing.

VII. Comparison With Other BMSs

The proposed MMC has been compared with the most common active BMS topologies to highlight its potentialities for the use with BEVs. Table V shows the hardware elements required as a function of the number of battery cells and compares the different BMSs in terms of size, cost, equalizing time, and efficiency. As shown in Table V, the capacitor-based methods have smaller energy losses in comparison with inductor/transformer-based and converter-based methods, but they have longer equalization time. The single switched capacitor method (SSC) has the smallest energy losses and its equalization time is acceptable compared with the switched capacitor (SC), double-tiered switched capacitor (DTSC), and modularized switched capacitor (MSC) methods [4].

On the other hand, multiwinding transformer (MWT) and multiswitched inductor (MSI) methods have a smaller equalization time than capacitor-based methods, but they are not suitable for Li-ion cells because they are working on the voltage difference between the cells. Moreover, MWT and MSI use a high number of windings and a bulky iron core, so they have large sizes and high magnetic losses. However, the single winding transformer (SWT) and single switch inductor (SSI) methods have faster equalization time and lower magnetic losses, but they require a more complex control. Additionally, the core of SWT must be changed to add one or more cells. Filtering capacitors are needed for SSI when a high switching frequency is needed. Buck–boost converter (BBC) methods have the smallest equalization time with acceptable energy losses compared with flyback converter (FbC) methods, Cuk converter (CC) methods, and ramp converter (RC) methods [5].

One of the primary advantages of the proposed MMC is to use the load current to balance the battery cells and using the same converter to drive the traction motor. These characteristics lead to balance the cells very quickly without extra energy losses in the auxiliary hardware required for conventional BMSs. The proposed topology do not use high-voltage and high-current switches, and therefore, the cost is significantly reduced. In the hardware design, each half-bridge converter and its driver is mounted on the battery modules so that the power cables and control wires are very short and light. As a result, the MMC has the smallest equalization time, limited energy losses with acceptable size and cost in comparisons with all the most common BMSs.

VIII. Conclusion

A new modular multilevel topology with embedded electrochemical cells for BEVs has been presented in this paper. This topology is based on a modular concept of multilevel half-bridge cells, with the aim of integrating active BMS into the converter structure. The results presented in the paper shows that this topology actively equalizes the cells and, hence, improves the battery life. The large number of levels of the output voltages strongly reduces the THD of motor currents, reducing power losses of the motor. The proposed converter is therefore a suitable candidate to eliminate the balancing circuits of the battery pack of electric vehicles enabling a new concept of battery cells directly embedded in the power converter. Numerical simulations with data of a real city car and experimental tests

TABLE V
COMPARISON OF THE PROPOSED MMC WITH DIFFERENT BMSS

Topology	L	C	SW	D	IC	Size	Cost	Equalising Time	Efficiency
SC	0	$n-1$	$2n$	0	0	+	+	±	+++
DTSC	0	n	$2n$	0	0	+	+	++	+++
SSC	0	1	$n+5$	0	0	++	++	+	+++
MSC	0	$n-1$	$2n+2m$	0	0	+	+	+	+++
MSI	$n-1$	0	$2n-2$	0	0	+	+	++	++
SSI	1	0	$2n$	$2n-2$	0	+	+	++	++
SWT	2	0	$n+6$	0	1	+	±	+	+
MWT	$n+1$	0	2	0	1	±	±	+	+
BBC	1	1	$n+7$	0	0	+	+	+++	+++
CC	$2n-2$	$n-1$	$2n-2$	0	0	+	+	++	++
FbC	$2n$	1	$2n$	0	n	±	±	+	+
RC	$n/2$	n	n	n	1	±	±	+	+
MMC	**6**	**0**	**2*n***	**0**	**0**	+	+	+++	+++

L: number of inductors, C: number of capacitors, D: number of diodes, SW: number of switches, IC: number of iron cores, n: number of cells, m: number of SMs. +++ = Excellent, ++ = Very good, + = Good, ± = Satisfactory.

on a laboratory prototype confirm the technical features of the converter's topology presented.

APPENDIX A
DERIVATION OF (7)

The current flowing into any battery cell can be expressed in terms of the value of cell SOC and the cell capacity

$$i_{h,kt} = Q_{max}\frac{d\mathrm{SOC}_{h,kt}}{dt},\ \ h=1,...,n,\ \ k=a,b,c$$
$$i_{h,kb} = Q_{max}\frac{d\mathrm{SOC}_{h,kb}}{dt},\ \ h=1,...,n,\ \ k=a,b,c. \quad \text{(A1)}$$

Considering ideal switches, the instantaneous active power balancing on both sides of each SM of the top and bottom arms yields

$$p_{h,kt} = i_{kt}v_{h,kt} = i_{h,kt}V_{\mathrm{cell}} = \left(Q_{max}\frac{d\mathrm{SOC}_{h,kt}}{dt}\right)V_{\mathrm{cell}}$$
$$p_{h,kb} = i_{kb}v_{h,kb} = i_{h,kb}V_{\mathrm{cell}} = \left(Q_{max}\frac{d\mathrm{SOC}_{h,kb}}{dt}\right)V_{\mathrm{cell}}. \quad \text{(A2)}$$

The instantaneous power of each arm is equal to the summation of the instantaneous active power of each SM within that arm

$$p_{kt} = \sum_{h=1}^{n} p_{h,kt} = i_{kt}\sum_{h=1}^{n} v_{h,kt} = \left(Q_{max}\sum_{h=1}^{n}\frac{d\mathrm{SOC}_{h,kt}}{dt}\right)V_{\mathrm{cell}}$$
$$p_{kb} = \sum_{h=1}^{n} p_{h,kb} = i_{kb}\sum_{h=1}^{n} v_{h,kb} = \left(Q_{max}\sum_{h=1}^{n}\frac{d\mathrm{SOC}_{h,kb}}{dt}\right)V_{\mathrm{cell}}. \quad \text{(A3)}$$

By substituting (8) into (A3), the instantaneous power of each arm can be expressed as a function of the average SOC for the top and bottom arm of the phase k

$$i_{kt}\sum_{h=1}^{n} v_{h,kt} = i_{kt}v_{kt} = n\,Q_{\max}V_{\mathrm{cell}}\frac{d\overline{\mathrm{SOC}}_{kt}}{dt}$$
$$i_{kb}\sum_{h=1}^{n} v_{h,kb} = i_{kt}v_{kb} = n\,Q_{\max}V_{\mathrm{cell}}\frac{d\overline{\mathrm{SOC}}_{kb}}{dt}. \quad \text{(A4)}$$

REFERENCES

[1] The International Organization of Motor Vehicle Manufacturers,. (2014, Sep. 4). "World Motor Vehicle Production by Country and type. [Online]. Available: http://www.oica.net/wp-content/uploads/total-2013-2.pdf

[2] J. O. Estima and A. J. Marques Cardoso, "Efficiency analysis of drive train topologies applied to electric/hybrid vehicles," *IEEE Trans. Veh. Technol.*, vol. 61, no. 3, pp. 1021–1031, Mar. 2012.

[3] S. D'Arco, L. Piegari, and P. Tricoli, "A modular converter with embedded battery cell balancing for electric vehicles," in *Proc. Elect. Syst. Aircraft, Railway Ship Propulsion*, Bologna, Italy, Oct. 16–18, 2012, pp. 1–6.

[4] M. Daowd, M. Antoine, N. Omar, P. Van Den Bossche, and J. Van Mierlo, "Single switched capacitor battery balancing system enhancements," *Energies*, vol. 6, no. 4, pp. 2149–2174, Apr. 2013.

[5] M. Daowd, M. Antoine, N. Omar, P. Van Den Bossche, and J. Van Mierlo, "Passive and active battery balancing comparison based on MATLAB simulation," in *Proc. IEEE Vehicle Power Propulsion Conf.*, Chicago, IL, USA, Sep. 6–9, 2011, pp. 1–7.

[6] W. Qian, H. Cha, F. Z. Peng, L. M. Tolbert, "55-kW variable 3X DC-DC converter for plug-in hybrid electric vehicles," *IEEE Trans. Power Electron.*, vol. 27, no. 4, pp. 1668–1678, Apr. 2012.

[7] L. M. Tolbert, J. N. Chiasson, K. J. McKenzie, and Z. Du, "Control of cascaded multilevel converters with unequal voltage sources for HEVs," in *Proc. IEEE Int. Electric Mach. Drives Conf.*, Madison, WI, USA, Jun. 1–4, 2003, vol. 2, pp. 663–669.

[8] K. Ilves, S. Norrga, L. Harnefors, and H. -P. Nee, "On energy storage requirements in modular multilevel converters," *IEEE Trans. Power Electron.*, vol. 29, no. 1, pp. 77–88, Jan. 2014.

[9] H. Akagi, "Classification, terminology, and application of the modular multilevel cascade converter (MMCC)," *IEEE Trans. Power Electron.*, vol. 26, no. 11, pp. 3119–3130, Nov. 2011.

[10] G. P. Adam, O. Anaya-Lara, G. M. Burt, D. Telford, B. W. Williams, and J. R. McDonald, "Modular multilevel inverter: pulse width modulation and capacitor balancing technique," *IET Power Electron.*, vol. 3, no. 5, pp. 702–715, Sep. 2010.

[11] M. Surprenant, I. Hiskens, and G. Venkataramanan, "Phase tracking locked loop control of inverters in a microgrid," in *Proc. IEEE Energy Convers. Congr. Expo.*, Phoenix, AZ, USA, Sep. 17–22, 2011, pp. 667–672.

[12] G. Ding, M. Ding, and G. Tang, "An Innovative modular multilevel converter topology and modulation control scheme for the first VSC-HVDC project in China," in *Proc. Power System Comput. Conf.*, Glasgow, U.K., Jul. 14–18, 2008, pp. 1–8.
[13] Q. Song, W. Liu, Z. Li, H. Rao, S. Xu, and L. Li, "A steady-state analysis method for a modular multilevel converter," *IEEE Trans. Power Electron.*, vol. 28, no. 8, pp. 3702–3713, Aug. 2013.
[14] M. H. Rashid, "Pulse width modulated inverters," in *Power Electronics Circuits, Drives and Applications*. 3rd ed., Upper Saddle River, USA: Prentice-Hall, 2013.
[15] X. Yang, J. Li, X. Wang, W. Fan, and T. Q. Zheng, "Circulating current model of modular multilevel converter," in *Proc. Asia-Pacific Power Energy Eng. Conf.*, Wuhan, China, Mar 25–28, 2011, pp. 1–6.
[16] Y. Zhang, Q. Ge, R. Zhang and Y. Du, "The control of arm currents and the parameters for modular multilevel converters," in *Proc. 15th Int. Conf. Elect. Mach. Syst.*, Sapporo, Japan, Oct. 21–24, 2012, pp. 1–6.
[17] Z. Li, P. Wang, Z. Chu, H. Zhu, Y. Luo, and Y. Li, "An inner current suppressing method for modular multilevel converters," *IEEE Trans. Power Electron.*, vol. 28, no. 11, pp. 4873–4879, Nov. 2013.
[18] A. Lesnicar and R. Marquardt, "An innovative modular multilevel converter topology suitable for a wide power range," in *Proc. IEEE Power Tech Conf.*, Bologna, Italy, Jun. 23–26 2003, vol. 3, pp. 1–6.
[19] L. Maharjan, S. Inoue, H. Akagi, and J. Asakura, "State-of-Charge (SOC)-balancing control of a battery energy storage system based on a cascade PWM converter," *IEEE Trans. Power Electron.*, vol. 24, no. 6, pp. 1628–1636, Jun. 2009.
[20] D. J. Deepti, and V. Ramanarayanan, "State of charge of lead acid battery," in *Proc. India Int. Conf. Power Electron.*, Chennai, India, Dec. 19–21, 2006, pp. 89–93.
[21] P. Moss, G. Au, E. Plichta, and J. P. Zheng, "An electrical circuit for modeling the dynamic response of li-ion polymer batteries," *J. Electrochem. Soc.*, vol. 155, pp. A986–A994, Oct. 2008.
[22] F. Feng, R. Lu, and C. Zhu Moo, "A combined state of charge estimation method for lithium-ion batteries used in a wide ambient temperature range," *Energies*, vol. 7, pp. 3004–3032, May 2014.
[23] K. S. Ng, C. S. Moo, Y. P. Chen, and Y. C. Hsieh, "Enhanced coulomb counting method for estimating state-of-charge and state-of-health of lithium-ion batteries," *Appl. Energy*, vol. 86, no. 9, pp. 1506–1511, 2009.
[24] R. Billinton and R. N. Allan, *Reliability Evaluation of Engineering Systems: Concepts and Techniques*, 2nd ed. New York, NY, USA: Plenum Press, 1992.
[25] S. D'Arco, L. Piegari, M. Quraan, and P. Tricoli, "AC battery charging in modular multilevel converters for electric vehicles," in *Proc. IET Int. Conf. Power Electron., Mach. Drives*, Manchester, U.K., Apr. 8–10, 2014, pp. 1–6.
[26] J. Yun, T. Yeo, and J. Park, "High efficiency active cell balancing circuit with soft switching technique for series-connected battery string," in *Proc. 28th IEEE Appl. Power Electron. Conf. Expo.*, Long Beach, CA, USA, Mar. 17–21 2013, pp. 3301–3004.

Mahran Quraan received the B.Sc. degree in electrical engineering from Birzeit University, Palestine, in 2008, and the M.Sc. degree in electrical power engineering from the University of Strathclyde, UK, in 2012, under a full scholarship from the "Palestinian Student Scholarship Scheme." He is currently working toward the Ph.D. degree at the School of Electronic, Electrical, and Systems Engineering, University of Birmingham, Birmingham, U.K., with a scholarship funded by Palestinian Telecommunication Group (PalTel), Samsung Advanced Institute of Technology, and the University of Birmingham.

He subsequently worked as a Teaching and Research Assistant in the Department of Electrical Engineering, Birzeit University. He then joined the Department of Electrical Engineering, Birzeit University, as a Faculty Member. His research interests include modular multilevel converters, battery management systems, protection and control of power systems, control of power converters, and ac machine drives.

Taejung Yeo received the B.S., M.S., and Ph.D. degrees from the Department of Metallurgical Science and Engineering, Seoul National University, Seoul, Korea, in 1993, 1995, and 2000, respectively.

He is currently a Research Staff of Samsung Advanced Institute of Technology, Gyunggi-do, Korea. His current research interest includes battery management technology of Electric Vehicle battery system based on intelligent data analysis.

Pietro Tricoli (M'06) was born in Naples, Italy, on September 8, 1978. He received the M.S. (*cum laude*) and Ph.D. degrees in electrical engineering from the University of Naples Federico II, Napoli, Italy, in 2002 and 2005, respectively.

He was a Visiting Scholar in the Department of Electrical and Computer Engineering, University of Wisconsin-Madison, Madison, in 2005. In 2006, he was also a Visiting Scholar in the Department of Electrical and Electronic Engineering, Nagasaki University, Nagasaki, Japan. From 2006 to 2011, he was a Postdoctoral Research Fellow with the Department of Electrical Engineering, University of Naples Federico II. He is currently a Lecturer of electrical power and control in the School of Electronic, Electrical, and Systems Engineering, University of Birmingham, Birmingham, U.K. He is the author of more than 60 scientific papers published in international journals and conference proceedings. His research interests include the modeling of storage devices for road electric vehicles, railways, and rapid transit systems, the wind and photovoltaic generation, and the modeling and control of multilevel converters.

Dr. Tricoli is a Member of the IEEE Industrial Electronics Society. He is the Web & Publication Chair of the International Conference on Clean Electrical Power. He is a Registered Professional Engineer in Italy.